ANTIOXIDANTS & REDOX SIGNALING
Volume 15, Number 3, 2011

DOI: 10.1089/ars.2010.3829

ORIGINAL RESEARCH COMMUNICATION

A Key Role for NOX4 in Epithelial Cell Death During Development of Lung Fibrosis

Stephanie Carnesecchi,[1,2] Christine Deffert,[2] Yves Donati,[1,2] Olivier Basset,[2] Boris Hinz,[3] Olivier Preynat-Seauve,[2,4] Cecile Guichard,[5] Jack L. Arbiser,[6] Botond Banfi,[7] Jean-Claude Pache,[2] Constance Barazzone-Argiroffo,[1,2,*] and Karl-Heinz Krause [2,4,*]

Abstract

The pathogenesis of pulmonary fibrosis is linked to oxidative stress, possibly generated by the reactive oxygen species (ROS) generating NADPH oxidase NOX4. Epithelial cell death is a crucial early step in the development of the disease, followed only later by the fibrotic stage. We demonstrate that in lungs of patients with idiopathic lung fibrosis, there is strong expression of NOX4 in hyperplastic alveolar type II cells. ***Aim:*** To study a possible causative role of NOX4 in the death of alveolar cells, we have generated NOX4-deficient mice. ***Results:*** Three weeks after administration of bleomycin, wild-type (WT) mice developed massive fibrosis, whereas NOX4-deficient mice displayed almost normal lung histology, and only little Smad2 phosphorylation and accumulation of myofibroblasts. However, the protective effects of NOX4 deficiency preceded the fibrotic stage. Indeed, at day 7 after bleomycin, lungs of WT mice showed massive increase in epithelial cell apoptosis and inflammation. In NOX4-deficient mice, no increase in apoptosis was observed, whereas inflammation was comparable to WT. *In vitro*, NOX4-deficient primary alveolar epithelial cells exposed to transforming growth factor-β_1 did not generate ROS and were protected from apoptosis. Acute treatment with the NOX inhibitors also blunted transforming growth factor-β_1–induced apoptosis. ***Conclusion:*** ROS generation by NOX4 is a key player in epithelial cell death leading to pulmonary fibrosis. *Antioxid. Redox Signal.* 15, 607–619.

Introduction

IDIOPATHIC PULMONARY FIBROSIS (IPF) is a progressive, devastating lung disease in humans. Lung fibrosis can be observed in response to different types of damage to the alveoli (39, 50). However, in lung biopsies of IPF, the initial injury is found principally in epithelial cells (23). In reaction to epithelial destruction, there is an impaired re-epithelialization, myofibroblast formation, generation of fibroblastic foci, and ultimately fibrotic scars (22). Over time, pulmonary fibrosis also leads to pulmonary hypertension (33). While the sequence of pathophysiological changes in IPF is relatively well studied, the etiological causes are still unknown. Reactive oxygen species (ROS) have been involved in the disease, although an antioxidant treatment used in a multicenter patient trial showed modest beneficial effects (11, 12, 18).

ROS generation by NOX family NADPH oxidases might be implicated in the pathogenesis of IPF (2, 16, 27). Seven genes for

Innovation

Epithelial cell death is a crucial step in the development of lung fibrosis. Reactive oxygen species generating NADPH oxidase NOX4 has been shown to participate in mechanisms of fibroblast/myofibroblast differentiation in lung fibrosis. Our study is the first investigation of bleomycin-induced lung fibrosis in NOX4-deficient mice. We demonstrate that the reactive oxygen species generating NOX4 plays an important role in the pathogenetic steps of lung fibrosis preceding fibroblast/myofibroblast differentiation. More specifically, NOX4 is crucial for epithelial cell apoptosis in response to bleomycin *in vivo* and in response to TGF-β_1 *in vitro*.

Departments of [1]Pediatrics and [2]Pathology and Immunology, Medical School, University of Geneva, Geneva, Switzerland.
[3]CIHR Group in Matrix Dynamics, University of Toronto, Toronto, Canada.
[4]Departement of Genetic and Laboratory Medicine, Geneva University Hospitals, Clichy, France.
[5]INSERM, U773, Centre de Recherche Biomédicale Bichat-Beaujon, Clichy, France.
[6]Department of Dermatology, Emory University School of Medicine, The Atlanta Veterans Administration Medical Center, Atlanta, Georgia.
[7]Department of Anatomy and Cell Biology and Center for Gene Therapy, University of Iowa City, Iowa.
*These two authors contributed equally to this work.

NOX enzymes are known (3). NOX enzymes are involved in the development of several diseases (3). Of particular interest for lung fibrosis are NOX2, expressed in inflammatory cells, and NOX4, expressed in fibroblasts and in different types of epithelial cells. Two recent studies suggested increased expression of NOX4 in fibroblasts from IPF patients (2, 16).

Bleomycin-induced lung fibrosis is a widely used mouse model of IPF. This model is thought to be recapitulating key aspects of the human disease, in particular epithelial cell death, myofibroblast activation, and lung scarring (30, 31). There are three notable differences with human disease: (i) an important inflammatory phase is observed in the mouse model, but to a much lesser extent in human IPF; (ii) pulmonary hypertension can be observed in human IPF, but not in the mouse model; (iii) fibrotic foci are described only in humans. Similarly as seen for human IPF, there is an implication of ROS in the pathomechanism of bleomycin-induced fibrosis. ROS may contribute to the activation of fibrogenic molecules such as transforming growth factor (TGF)-β_1 (21), which is a potent mediator of alveolar epithelial injury and myofibroblast activation (36). ROS have also been suggested to regulate TGF-β_1 down-stream signaling (20, 21).

NOX2-deficient mice show a moderate protection from bleomycin-induced lung fibrosis (27); however, extrapolation to human IPF is difficult as inflammation might not be as prominent in human as compared to mice. NOX4-deficient mice have not been investigated in a model of lung fibrosis so far; however, instillation of siRNA directed against NOX4 showed beneficial effects in bleomycin-induced fibrosis (16). These effects were attributed to an impaired TGF-β_1 signaling in NOX4-repressed fibroblasts, leading to decreased myofibroblast formation and collagen deposition.

Here we discovered a novel role for NOX4 in death of alveolar epithelial cells. We showed that NOX4 was highly expressed in hyperplastic alveolar type II cells in IPF patients. We demonstrated that NOX4-deficient mice are protected from bleomycin-induced pulmonary fibrosis through modulation of epithelial cell death *in vivo*. NOX4 deficiency as well

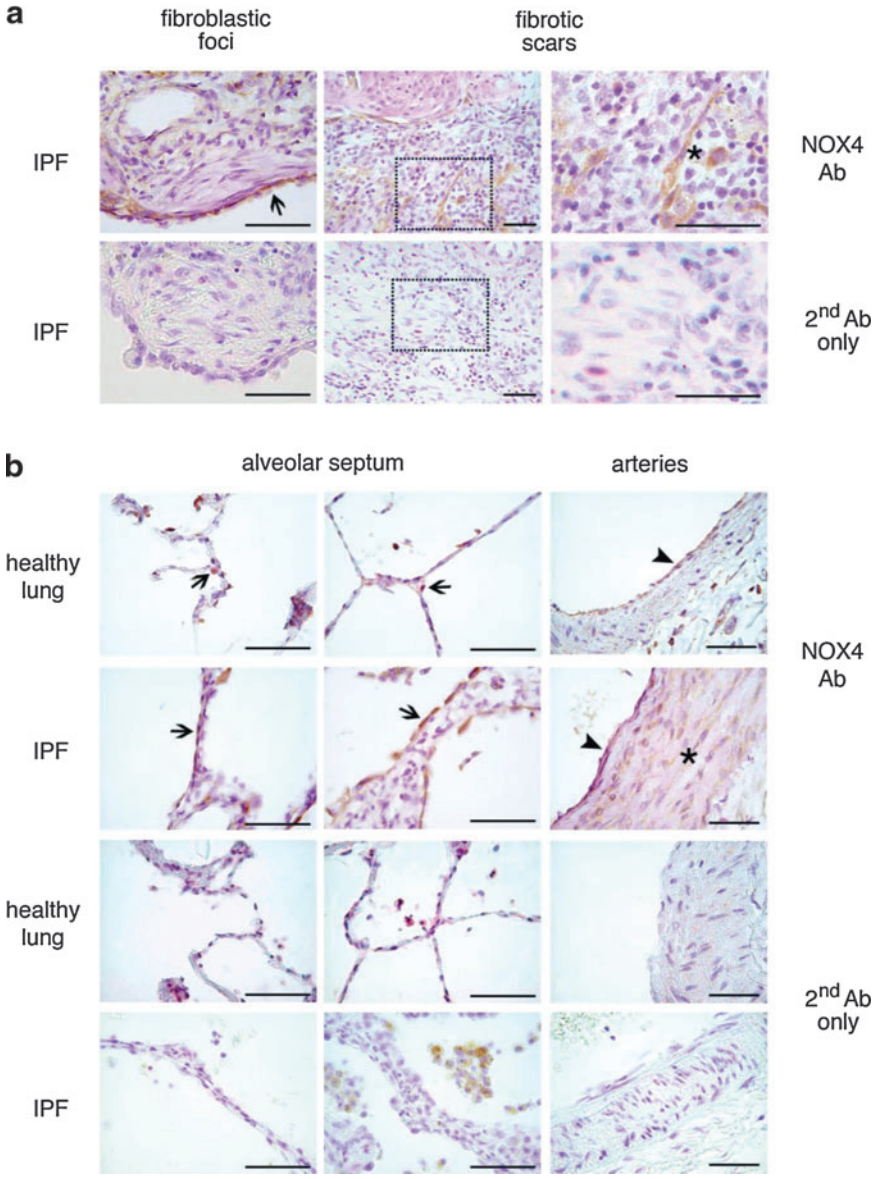

FIG. 1. Immunohistological analysis of NOX4 expression in idiopathic pulmonary fibrosis (IPF) and in healthy lungs. **(a)** IPF lung tissue was analyzed for NOX4 by immunohistochemistry. *Upper panels* show a fibroblastic focus (recent lesion) and a fibrotic scar (older lesion; two different magnifications). Boxes represent magnified regions of fibrotic scars. *Arrow* points the regenerative NOX4-positive alveolar epithelium lying adjacent to a fibrotic focus (which itself is NOX4-negative). *Asterisk* indicates a NOX4-positive fibroblast in a fibrotic scar. *Lower panels* are stained with secondary antibody only (Ab). Scale bars, 50 μm. **(b)** Different structures from healthy lungs (*panels* on *top line* and *third line*) and from IPF patients (*panels* on *second* and *fourth line*) stained with NOX4 antibody (*top line* and *second line*) or with secondary antibody only (*third* and *fourth lines*). In both, healthy and in IPF lungs, the anti-NOX4 antibody stained pulmonary epithelial cells (*arrows*) and endothelial cells (*arrowhead*). Medial smooth muscle cells (*asterisk*) located in the pulmonary arteries were positive only in IPF samples. Note the presence of hemosiderin-laden macrophages in the alveoli of IPF lungs stained with the secondary antibody only. Scale bars, 50 μm. (To see this illustration in color the reader is referred to the web version of this article at www.liebertonline.com/ars).

as NOX4 inhibitors prevent TGF-β_1-induced cell death *in vitro*.

Some of these results have been previously reported in the form of abstract (7).

Results

NOX4 is highly expressed in alveolar epithelial cells of IPF lungs

To study expression of NOX4, we have performed immunohistochemistry with a NOX4 antibody in sections of IPF and of healthy lungs (Fig. 1a, b). Negative controls were obtained by staining lung sections with secondary antibody only (Fig. 1a, b). Fibroblastic foci, which are relatively early lesions in the fibrosis stage, did not contain NOX4-expressing fibroblasts, even if the adjacent alveolar epithelium was clearly NOX4 positive (Fig. 1a). Within fibroblastic scars, which are later stage fibrotic lesions, some, but not all, of the fibroblasts expressed NOX4 (Fig. 1a). Thus, NOX4 expression in typical IPF lesions is variable and appears to be a late—rather than early—event.

We next analyzed other lung structures in healthy and IPF lungs (Fig. 1b). In healthy lungs, NOX4 was found in alveolar epithelial cells and in endothelial cells. In IPF lungs, the most striking finding was a strong staining of the hyperplastic alveolar type II cells. Strong NOX4 staining was also found in the thickened media of IPF lung arteries (33). Thus, NOX4 is expressed in alveolar epithelium and pulmonary vascular endothelium under physiological conditions, and in addition in the vascular media of IPF lungs. In addition, there is variable expression of NOX4 in late fibrotic lesions.

NOX4 deficiency decreases bleomycin-induced lung fibrosis

Both epithelial cell death and development of lung fibrosis are reproduced in the mouse model of bleomycin-induced lung fibrosis. To test the causal involvement of NOX4 in these pathophysiological mechanisms, we have generated NOX4-deficient mice by homologous recombination (Fig. 2a–c) and speed back-crossing into a pure C57Bl/6 genetic background (25). In these mice, as expected, NOX4 mRNA was not expressed in any tissue; examples shown are spleen, kidney, and lung (Fig. 2d). Similarly, there was no NOX4 protein detected in lungs from NOX4-deficient mice, whereas NOX4 expression was conserved in NOX1- and NOX2-deficient mice (Fig. 2e). In addition, bleomycin-induced ROS production was blunt in NOX4-deficient mice as measured by dihydroethidium (DHE) staining (Fig. 2f). Further, these mice were healthy and did not display any spontaneous phenotype, besides a moderate tendency for accelerated increase in weight (data not shown).

We have compared the impact of bleomycin on the development of pulmonary fibrosis in wild-type (WT) and NOX4-deficient mice. WT mice showed massive weight loss in response to bleomycin, whereas NOX4-deficient mice rapidly returned to normal after a minor initial decrease in weight (Fig. 3a). Histochemical analysis (Masson's Trichrome staining) demonstrated that WT mice developed severe pulmonary fibrosis in response to bleomycin, in contrast to few fibrotic lesions that were observed in NOX4-deficient mice (Fig. 3b). These results were quantitatively confirmed by analysis of total pulmonary collagen content (Fig. 3c) and procollagen IIIa mRNA levels (Fig. 3d). Thus, NOX4-deficient mice developed decreased pulmonary fibrosis in response to bleomycin.

NOX4 does not modulate inflammation induced by bleomycin

Inflammation is observed during the initial phase of bleomycin-induced pulmonary fibrosis and thought to contribute to fibrosis development (49). To investigate whether the protection provided by NOX4 deficiency is linked to inflammation, we investigated bronchoalveolar lavage fluid (BALF) for cell content (Fig. 4a–d) and levels of selected cytokines (Fig. 4e, f). None of these parameters was different between WT and knock-out animals. Note also that no significant changes were observed in the following inflammatory markers: MIP1α, RANTES, MIP-2, TNF, IL-10, and IFN (data not shown). Taken together, this suggests that NOX4 does not contribute to the pathogenesis of pulmonary fibrosis through modulation of inflammation.

Accumulation of myofibroblasts and phosphorylation of Smad2 induced by bleomycin depends on NOX4

Accumulation of myofibroblasts, to a large extent driven by TGF-β_1 signaling (13, 36), is a hallmark of advanced and progressing lung fibrosis in response to bleomycin. Activation of transcription factors of the Smad family, in particular of Smad2 and Smad3, is one of the major TGF-β_1-dependent signals (28, 36, 38). This activation occurs through phosphorylation by the TGF-β_1 receptor, which is a serine/threonine kinase (32). Marked increase in Smad2 phosphorylation was observed in lung homogenates of WT mice exposed for 21 days to bleomycin. In contrast, the levels of phospho-Smad2 in NOX4-deficient mice did not increase and were similar to saline controls (Fig. 5a). To investigate whether NOX4 is important for myofibroblast accumulation, we performed immunohistochemistry using an antibody against α-smooth muscle actin (α-SMA), the hallmark of myofibroblasts (17, 44). In saline-treated mice (both WT and NOX4-deficient), predominantly smooth muscle cells of blood vessels were stained by the antibody. In bleomycin-treated WT mice, fibroblasts present in pulmonary parenchyma were strongly labeled (Fig. 5b), indicating the massive accumulation of myofibroblasts. In contrast, only a very low parenchymal labeling was observed in NOX4-deficient mice after bleomycin exposure (Fig. 5b). Of note, myofibroblasts were seen in all sections in the media of the vessels.

In addition to Smad signaling, activation of MAP kinases has been suggested to contribute to lung fibrosis after bleomycin treatment (1). Consequently, we analyzed phosphorylation of ERK, JNK, and p38 MAP kinases in lung homogenates, 21 days after bleomycin exposure. In WT mice, both ERK and JNK were phosphorylated, whereas p38 phosphorylation was unchanged. Interestingly, bleomycin-induced phosphorylation of ERK and JNK was not altered in NOX4-deficient lungs (Fig. 5c; JNK phosphorylation at day 7 after bleomycin was also not affected by NOX4 deficiency; data not shown). Thus, bleomycin-induced Smad phosphorylation and accumulation of myofibroblasts depends on NOX4.

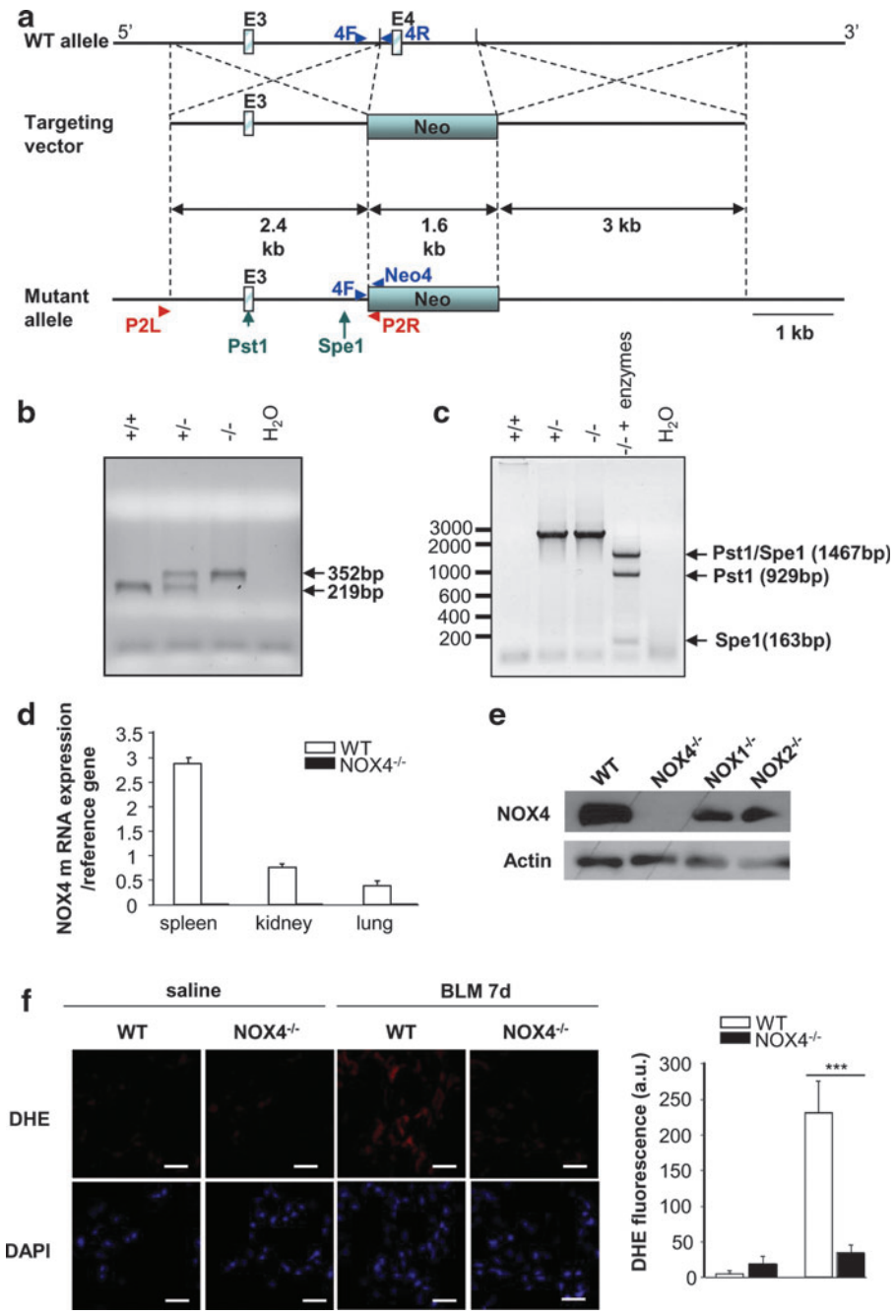

FIG. 2. Generation and characterization of global NOX4-deficient mice. (a) Diagram of the targeting vector (*middle*) designed to replace the *Hin*dIII fragment containing exon 4 (E4 = 85pb) of the *NOX4* gene in the wild-type (WT) allele (*top*) with a pGK-neo cassette (Neo). The predicted mutant allele generated by homologous recombination is shown (*bottom*). **(b)** Multiplex polymerase chain reaction (PCR) analysis for genotyping. Genomic DNAs obtained from F2 offspring ($^{+/+}$, WT; $^{+/-}$, heterozygote; $^{-/-}$, homozygote) were amplified using primer sequences (4F, 4R, and Neo4R) located near the deleted region (4F, 5′-TCA TGA CAG TTG GGG ACA AA-3′; 4R, 5′-TTG AAA ATT CAA CAC AAG TCT CC-3′; Neo4R, 5′-AAC GTC GTG ACT GGG AAA AC-3′). **(c)** PCR analysis to verify the homologous recombination. Genomic DNA obtained from F2 offspring ($^{+/+}$, WT; $^{+/-}$, heterozygote; $^{-/-}$, homozygote) was amplified using primer sequences (P2R and P2L) located upstream the targeting vector and in the pGK-neo cassette (P2R, 5′-CAA CTT AAT CGC CTT GCA GCA CAT C-3′; P2L, 5′-TGG AGG GAC AAG TTC TGA TAG CAG T-3′). The PCR products were then digested with *Pst*I and *Spe*I, marked as *arrows* in the mutant allele. **(d)** Expression of NOX4 mRNA in spleen, kidney, and lung (real-time PCR). Primers were designed to span exon 4–5 (4-5F, 5′-TCC CTA GCA GGA GAA CAA GAA-3′; 4-5R, 5′-TTG CTG CAT TCA GTT CAA GG-3′). **(e)** Lung lysates from WT and NOX4, NOX2-, and NOX1-deficient mice were analyzed by Western blot for NOX4. *β*-actin was used to control equal loading. **(f)** Representative fluorescent images of dihydroethidium (DHE)-loaded lungs sections. Reactive oxygen species (ROS) generation was measured by analyzing DHE staining (red) in lungs of WT and NOX4-deficient ($NOX4^{-/-}$) after saline or bleomycin (BLM) treatment at day 7. All nuclei of lung sections were stained with 4′,6′-diamidino-2-phenylindole (DAPI). Scale bars, 100 μm. Fluorescence intensity was quantified in whole lung sections; bars represent the mean ± standard error of the mean ($n = 3$ mice for each group; $^{***}p < 0.001$). (To see this illustration in color the reader is referred to the web version of this article at www.liebertonline.com/ars).

NOX4 is crucial in bleomycin-induced alveolar epithelial cell death

Next, we investigated a crucial proximal step in the pathogenesis of lung fibrosis, namely, epithelial cell apoptosis (22, 43). To this end, we first analyzed the time course of lung cell death by TUNEL staining in WT and NOX4-deficient mice (Fig. 6a). Instillation of saline had no or only minor effects on the number of TUNEL-positive cells up to 20 days either in WT or in NOX4-deficient mice. Instillation of bleomycin in WT mice led to a massive increase in TUNEL-positive cells during the first 2 weeks, returning to baseline levels after 3 weeks. In contrast, no significant increase in TUNEL-positive cells was observed in NOX4-deficient mice. Note that the differences between bleomycin-treated WT and NOX4-deficient mice were statistically significant ($p < 0.01$ on days 2 and 7, and $p < 0.05$ on day 12). Prevention of apoptosis by NOX4 deficiency

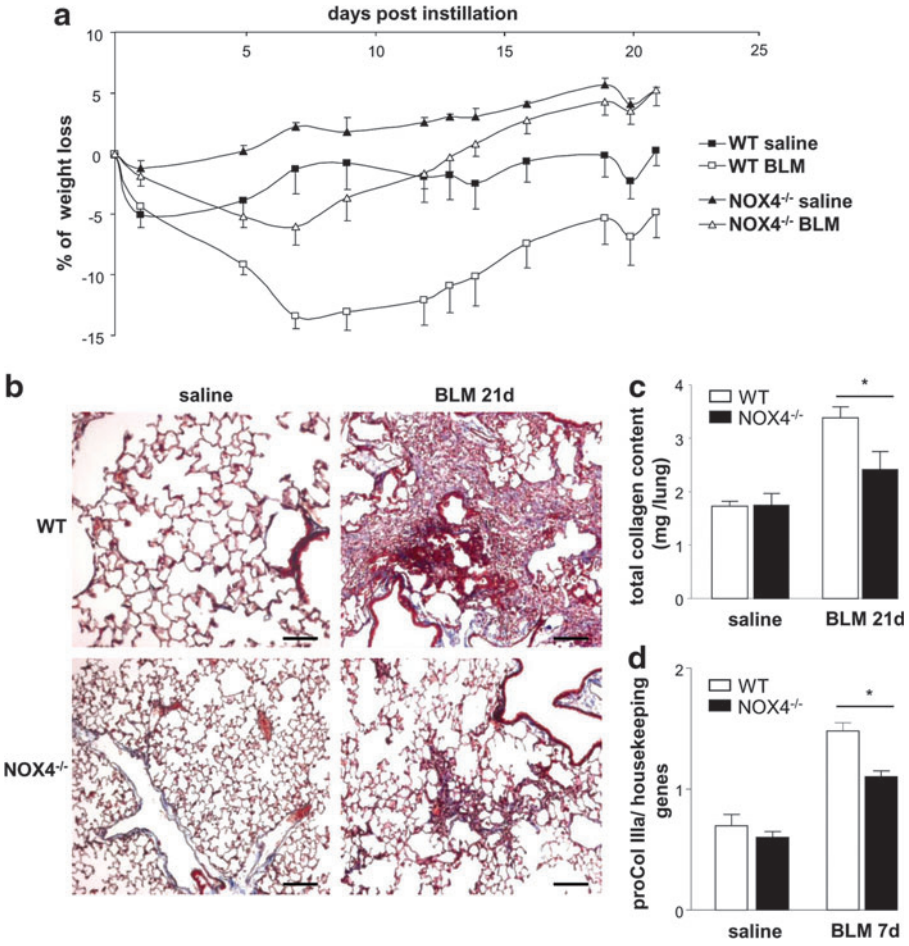

FIG. 3. NOX4-deficient mice are protected from BLM-induced lung fibrosis. **(a)** WT and NOX4-deficient mice ($NOX4^{-/-}$) were administered BLM at day 1 and weighed every 3 days during 21 days. Values are expressed as percent weight loss ($n=6$). The weight difference between WT mice with or without BLM, as well as the difference between WT and NOX4-deficient mice after BLM was significant by two-way analysis of variance ($p<0.001$). **(b)** Masson's trichrome staining of lung sections from WT and NOX4-deficient mice, at day 21. Scale bars, 100 μm. **(c)** Total collagen content was measured at day 21 by Sircol assay, ($n=10$); $^{*}p<0.05$. **(d)** Lung expression of pro-collagen IIIa mRNA measured by real-time PCR at day 7 ($n=5$). $^{*}p<0.05$. (To see this illustration in color the reader is referred to the web version of this article at www.liebertonline.com/ars).

was also observed by analyzing cleaved caspase-3 (Fig. 6b). To understand the temporal relationship between the epithelial cell apoptosis occurring in bleomycin-treated WT and the subsequent development of fibrosis, we analyzed the alveolar perimeter (a sensitive measure of lung fibrosis) as a function of time after bleomycin exposure. Bleomycin did not affect this parameter at day 7 (i.e., when maximum apoptosis occurs), but only at later time points (Supplementary Fig. S1; Supplementary Data are available online at www.liebertonline.com/ars). Thus, in the bleomycin model, epithelial cell apoptosis precedes the development of fibrosis.

To identify the type of cells undergoing cell death, we performed costaining of lung sections with TUNEL and cell type-specific markers (Fig. 6c). TUNEL-positive cells in WT mice were negative for the endothelial cell marker, but positive for alveolar epithelial type I and type II cell markers. Thus, NOX4 is essential for bleomycin-induced death of alveolar epithelial cells.

We also investigated NOX4 expression in lung homogenates of WT mice after bleomycin exposure (day 7). Interestingly, we observed a decrease in NOX4 expression 2.6 ± 0.39 in saline-treated mice, as compared to 1.03 ± 0.04 in bleomycin-treated mice; $p=0.02$. This most likely reflects the apoptotic loss of NOX4-expressing alveolar epithelial cells. As whole lung homogenates are a crude mixture of many cells types, precise information about the relationship between NOX4 expression and apoptosis in alveolar epithelial cells requires the work with primary cells.

NOX4 deficiency and acute inhibition of NOX4 prevents TGF-β_1-induced cell death in primary alveolar epithelial cells

To further determine the relationship between NOX4 and cell death, we analyzed isolated primary epithelial type II cells. Death of alveolar epithelial cells in pulmonary fibrosis is thought to be mediated, at least in part, by TGF-β_1 (26). Stimulation of epithelial type II cells with TGF-β_1 increased NOX4 mRNA expression (Fig. 7a). Even more striking, NOX4 deficiency almost entirely blunted TGF-β_1-induced ROS generation (Fig. 7b). Analysis of cell death yielded interesting results. Stimulation with TGF-β_1 for 24 h increased significantly the number of TUNEL-positive alveolar epithelial type II cells from WT mice. By contrast, a much lower number of cells were positive when derived from NOX4-deficient mice under TGF-β_1 stimulation (Fig. 7c). This suggests that NOX4-dependent ROS generation contributes to TGF-β_1-induced death of epithelial type II cells.

To demonstrate that resistance to TGF-β_1 is not a chronic adaptation due to the knock-out, we investigated acute NOX4 inhibition using fulvene-5, a compound that inhibits NOX4

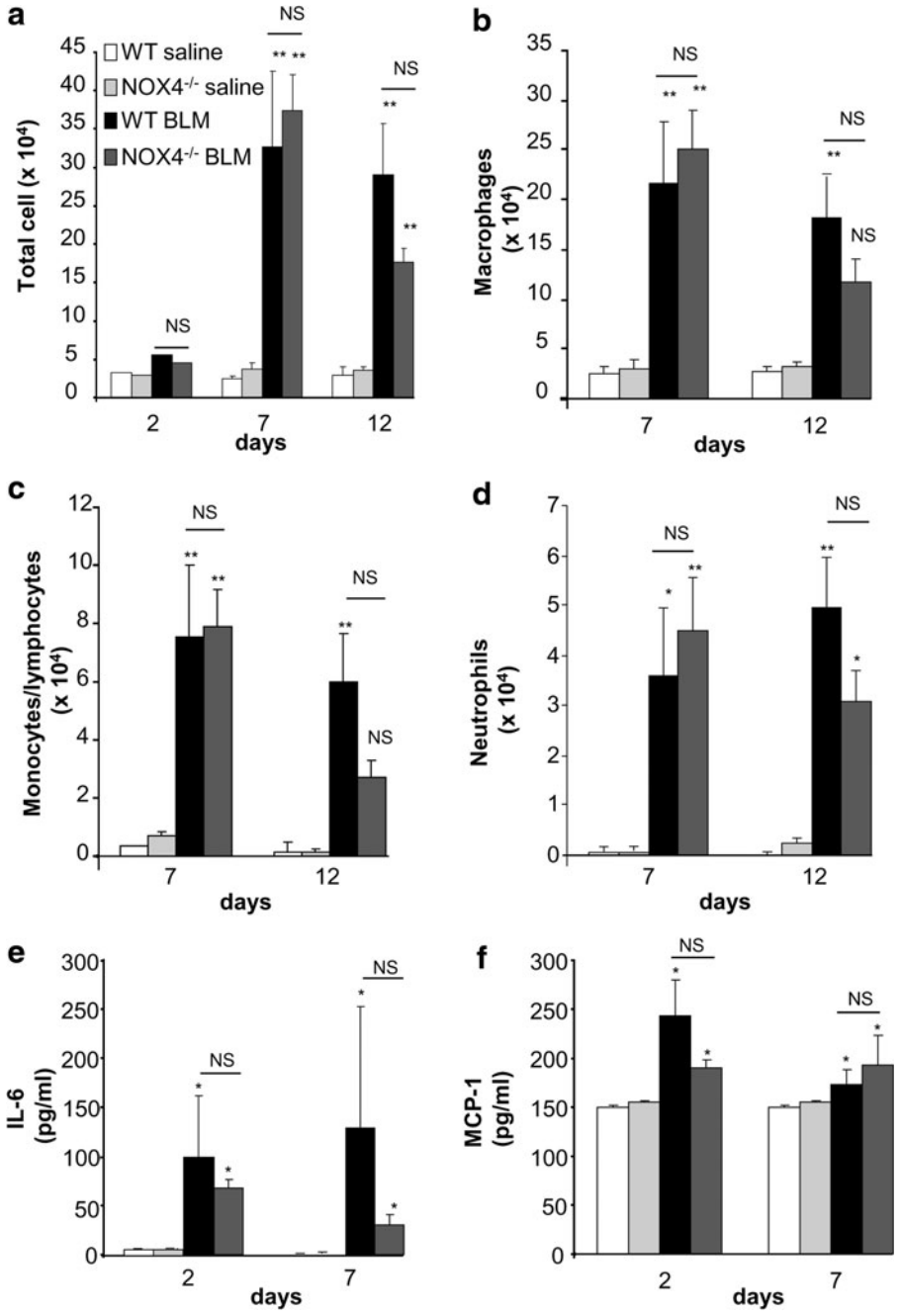

FIG. 4. NOX4 does not modulate BLM-induced inflammation. (a) Bronchoalveolar lavage was performed at the indicated time points and total cell counted. $p = \text{NS}$ (not significant), $^{**}p < 0.01$ BLM *versus* saline, $p = \text{NS}$ WT versus NOX4$^{-/-}$ in BLM condition ($n = 6$ mice in each group). **(b)** Macrophages, **(c)** monocytes/lymphocytes, and **(d)** neutrophils were counted separately on cytospin preparations. $^{*}p < 0.05$, $^{**}p < 0.01$ BLM *versus* saline. **(e)** IL-6 and **(f)** MCP-1 were measured in bronchoalveolar lavage supernatant, $^{*}p < 0.05$ BLM *versus* saline ($n = 3$ mice in each group).

and NOX2 (4), and GKT136901, a compound that inhibits NOX1 and NOX4 (24) (but not NOX2). Both inhibitors led to a decrease in TGF-β_1-induced apoptosis of epithelial type II cells (Fig. 7d). These results demonstrate that NOX4 activity is important for TGF-β_1-induced apoptosis in alveolar epithelium.

Discussion

In this study, using NOX4-deficient mice, we demonstrate that ROS generation by the NADPH oxidase NOX4 is crucial for the induction of alveolar epithelial cell death and the subsequent development of lung fibrosis. There is now strong evidence that epithelial cell death is a key event in the pathogenesis of lung fibrosis (22, 43). Indeed, apoptotic cells can be detected in lungs of IPF patients (23, 45), as well as in bleomycin-induced and TGF-β_1-induced mouse models of pulmonary fibrosis (19). Inhibitors of apoptosis diminish pulmonary fibrosis in mouse models (6, 47), whereas epithelial cell damage by transgenic expression of diphteria toxin is sufficient to induce pulmonary fibrosis in mice (41). Therefore, strategies aimed at preventing epithelial cell death are increasingly considered as crucial for future treatments of IPF.

ROS generation by NOX NADPH oxidases has a context-dependent impact on cell fate, and may contribute to cell

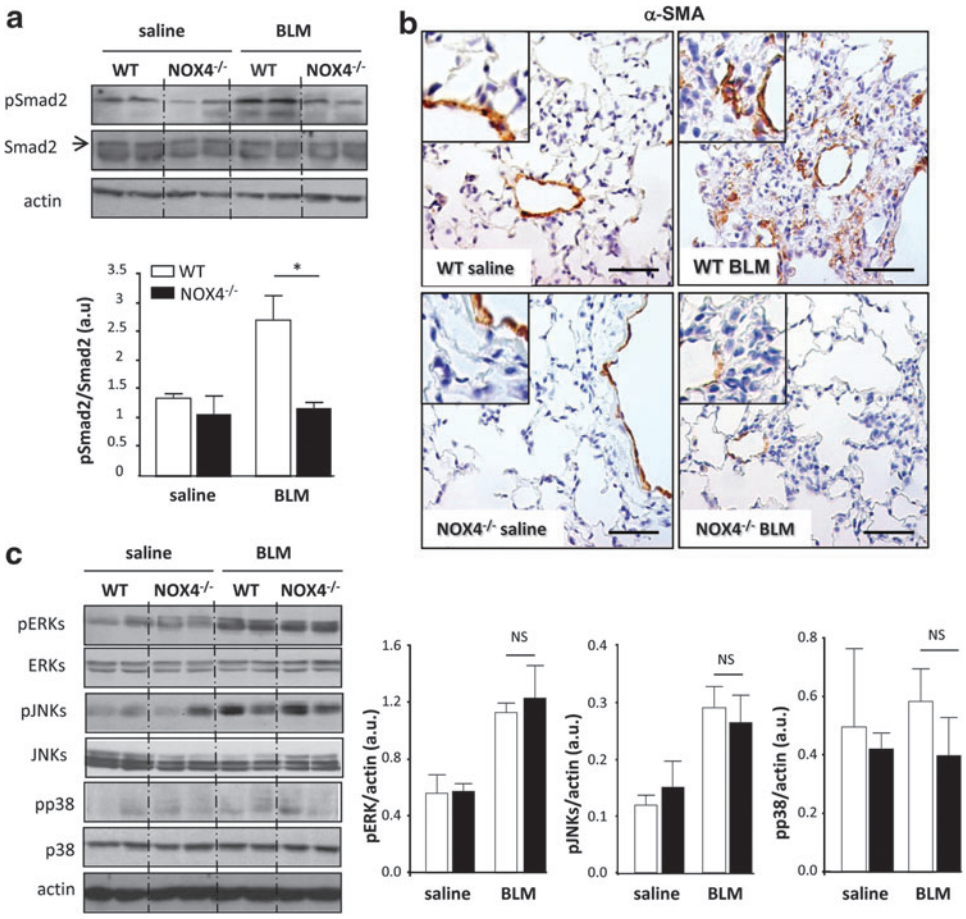

FIG. 5. NOX4 deficiency decreases transforming growth factor (TGF)-β_1 signaling and myofibroblast accumulation in response to BLM. Mice received intratracheal BLM and were sacrificed at day 21. **(a)** Lung lysates from WT and NOX4-deficient mice were analyzed by Western blot for phosphorylated and total Smad2 ($n=5$), $^{*}p<0.05$. **(b)** Myofibroblast accumulation was assessed by immunohistochemistry on WT and NOX4-deficient mice lung sections with an anti-α-smooth muscle (α-SMA), magnified in inset at top left. Scale bars, 50 μm. **(c)** Western blot for phosphorylated and total ERK, JNK, and p38 proteins quantified by densitometry ($n=5$), $p=$NS. β-actin was used to control equal loading. No significant changes were observed in MAP kinase activation pathways. Phosphorylated forms of the respective proteins are indicated by the prefix "p." (To see this illustration in color the reader is referred to the web version of this article at www.liebertonline.com/ars).

survival or to cell death (3). Even for the same NOX enzyme, such as NOX4, it can be involved in enhancement of cell growth (37), cell differentiation (10, 16), and in induction of cell death-independent cellular senescence (14). In the context of bleomycin-induced lung fibrosis *in vivo* and TGFβ_1-induced alveolar epithelial cell death *in vitro*, NOX4 is clearly involved in the induction of apoptosis (this study). Does it make sense from a biological point of view that NOX4 induces apoptosis in alveolar epithelial cells? In the same situation, NOX4 upregulation might be part of the response to danger signals leading to protective apoptosis as in viral infections (15). However, NOX4 regulation is likely to be more complex and its impact on cell fate might depend on expression levels: limited upregulation of NOX4 might have functions other than apoptosis (in particular cell signaling), whereas marked upregulation of NOX4 might lead to cell death. Mechanisms by which ROS contribute to cell death are complex: they include nonspecific cell damage as well as specific redox-sensitive pathways for cell signaling and transcriptional control (3). It has been suggested that ROS release from fibroblasts are the cause of epithelial cell death in pulmonary fibrosis (46). Our results do not favor this concept, but suggest cell autonomous effects of NOX4 in epithelial cells.

What is the relationship between lung fibrosis, NOX4, and TGF-β_1? Our data demonstrate that NOX4-derived ROS are crucial down-stream mediators of TGF-β_1-induced alveolar epithelial cell death. However, there are also indications that ROS might act upstream, contributing to TGF-β_1 expression and activation (21), raising the potential of a positive feedback loop between NOX4 and TGF-β_1 in lung fibrosis. It is likely that TGF-β_1 is not the only factor contributing to NOX4 expression in the bleomycin model. Indeed, NOX4 upregulation may be a part of cellular stress responses, such as endoplasmic reticulum stress (35). If this is true, NOX4 inhibition would be expected to be more efficient than TGF-β_1 inhibition in preventing the development of epithelial cell death and the subsequent fibrosis.

NOX4 deficiency did not affect all biological changes in response to bleomycin. In particular, it did not affect either the accumulation of inflammatory cells or the activation of MAP kinases ERK and JNK. Thus, MAP kinase activation in response to bleomycin might occur through activation of other ROS generating systems. Previous work from our laboratory has shown a key role of NOX1 in activation of MAP kinases by hyperoxia (8). This points to an interesting new concept in redox biology, namely, that different NOX enzymes may preferentially activate distinct signaling systems through mechanisms, including distinct subcellular localization (5) or distinct activation mechanisms (40). Note, however, that our results do not exclude a role of MAP kinases in lung fibrosis (1, 29) and epithelial cell death (8); they rather demonstrate that MAP kinase activation is not sufficient to cause sustained fibrosis in the absence of NOX4-dependent ROS generation.

NOX4 also contributes to TGF-β_1-induced α-SMA production and to the contractile function of human fibroblast-like

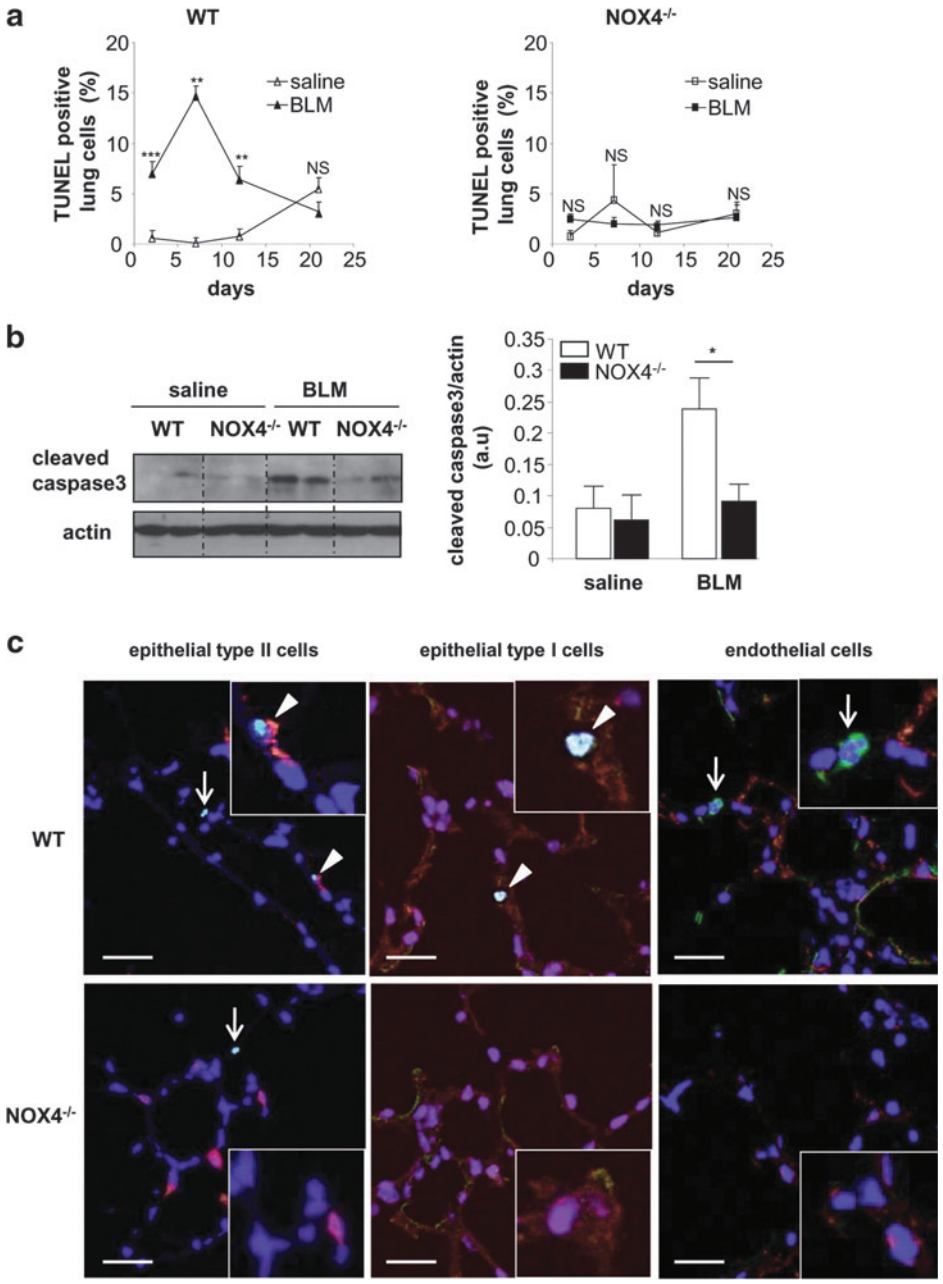

FIG. 6. NOX4 deficiency decreases BLM-induced death of alveolar epithelial cells. Mice receiving intratracheal saline or BLM were sacrificed at the indicated time points. **(a)** The number of TUNEL-positive cells at different time points (2, 7, 12, and 21 days) is expressed as percent of all nuclei counted in lung sections ($n = 3$–6 mice for each group): $p = $ NS, $^{**}p < 0.01$; $^{***}p < 0.001$ saline *versus* BLM. **(b)** Total lung lysates were blotted for cleaved caspase-3 (*left panel*) and quantified by densitometry (*right panel*; $n = 5$; day 7), $^{*}p < 0.05$. **(c)** Representative merged images (magnified in insets) of lung sections (day 7 after BLM) stained with TUNEL (green), DAPI (blue), and markers for epithelial type II cells (prosurfactant protein C, red), epithelial type I cells (T1-α, red), or endothelial cells (von Willebrand Factor, red). *White arrows* indicate TUNEL-positive cells that appear in *light blue* and *arrowheads* point the double-stained cells. Double-positive cells were observed only for TUNEL with the markers of epithelial type I and type II cells, but not with the marker of endothelial cells. Scale bars, 50 μm. (To see this illustration in color the reader is referred to the web version of this article at www.liebertonline.com/ars).

cells (2, 16). Therefore, our observation that, in human IPF, NOX4 is not detectable in myofibroblasts of early fibrotic foci (Fig. 1) is unexpected. This might suggest that early steps of myofibroblast formation in IPF require either no or only very low NOX4 activity and that NOX4 rather contributes to the development of the late fibrotic scar.

One of the key findings of our study, namely, the role of NOX4 in epithelial cell apoptosis, was also demonstrated using NOX4 inhibitors. This is important from a scientific point of view, as it proves that acute inhibition of NOX4 suffices to prevent apoptosis, and the resistance of NOX4-deficient epithelial type II cells to TGF-β_1-induced cell death was not due to chronic adaptation in NOX4-deficient animals. This is, however, also important in terms of perspectives for IPF treatment. NOX4 inhibition targets epithelial cell death (our study), but also later disease steps such as fibroblast activation (16), and theoretically even IPF-associated pulmonary hypertension (Fig. 1). NOX4 inhibitors are therefore a most promising treatment concept for this severe chronic disease for which no efficient therapies are known.

Materials and Methods

See the Supplementary Data for additional details on reagents and methods.

Immunostaining of lungs from control and IPF patients

Human lung biopsies of patient suffering from IPF and human normal control lungs were obtained in accordance to an approved protocol by the Institutional Ethics Committee

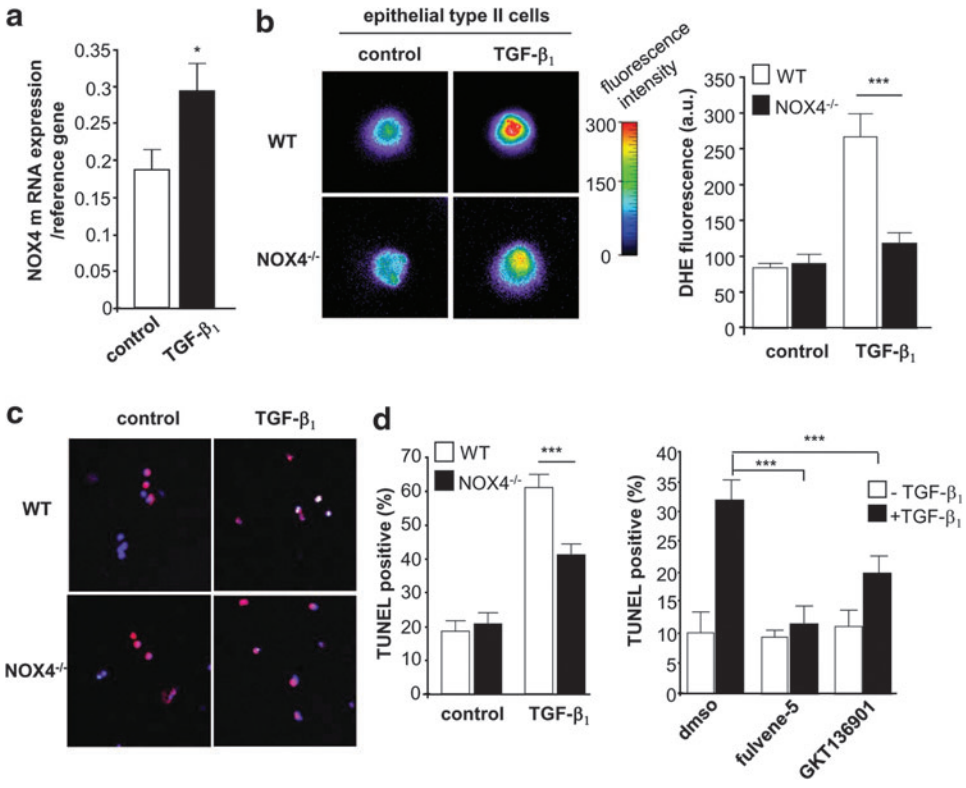

FIG. 7. NOX4 mediates TGF-β_1-induced ROS generation and death of epithelial type II cells. (a) Epithelial type II cells isolated from WT mice were incubated with or without TGF-β_1 and analyzed for NOX4 mRNA expression (real-time PCR). $^{*}p<0.05$. **(b)** TGF-β_1-induced ROS generation (DHE staining) in WT and in NOX4-deficient epithelial type II cells ($NOX4^{-/-}$); bars represent the mean ± standard error of the mean ($n=3$ mice for each group; $^{***}p<0.001$). **(c)** TGF-β_1-induced cell death (TUNEL staining) in WT and in $NOX4^{-/-}$ epithelial type II cells, $^{***}p<0.001$. **(d)** Epithelial type II cells isolated from WT mice were treated with DMSO, Fulvene-5 (5 μm), or GKT136901 (10 μm) and exposed to TGF-β_1 for 6 h. $^{***}p<0.001$ cells exposed to TGF-β_1 and NOX inhibitors compared to cells treated with TGF-β_1 and DMSO. (To see this illustration in color the reader is referred to the web version of this article at www.liebertonline.com/ars).

of Geneva. Paraffin-embedded sections of lung fixed in 4% paraformaldehyde (PFA) were stained with an anti-NOX4 polyclonal antibody (dilution 1/500; Novus Biologicals) (48) followed by an incubation with a biotinylated goat anti-rabbit Ig (1/100; Vector Laboratories). This reaction was developed using a horseradish peroxidase-avidin/biotin complex solution (1:100; Vector Laboratories) and diaminobenzidine (Invitrogen) before counterstaining with cresyl violet. Negative controls were obtained by incubating the sections with a biotinylated goat anti-rabbit Ig only (1/100; Vector Laboratories). In some control experiments, isotype controls were used, which yielded the same results (data not shown). Endogenous peroxidases were blocked by adding H_2O_2 and lung sections were subjected to heat-induced epitope retrieval for 15 min in 0.01 *M* citrate buffer (pH 6.0).

Generation of NOX4-deficient mice and speed back-cross

Embryonic stem cell clones Sv129 NOX4 (IIIG1 and IVA4) were thawed, plated on mitomycin C-inactivated mouse embryonic fibroblasts, and cultivated in Knockout D-MEM (Gibco Inc.) supplemented with leukocyte inhibitory factor and 15% fetal bovine serum (PAN Biotech GmbH). Cells were injected in one session each into C57Bl/6-derived blastocysts. For this purpose, 8-week-old C57Bl/6 female mice were naturally mated to C57Bl/6 breeder males (Charles River). Injections were performed using day 3.5 blastocysts obtained by cultivating day 3.5 morulae overnight at 37°C. Injected blastocysts were transferred into the uterus of pseudopregnant B6CBAF1 females (Charles River). The animals were kept in individually ventilated cages. Generation of knock-out embryonic stem cells as well as blastocyst injection and transfer were performed by PolyGene.

Speed-back cross into a C57Bl/6 background was performed as described (25). Briefly, polymerase chain reaction (PCR) was performed with genomic DNA as template. Three microsatellite marker loci per chromosome were amplified using appropriate PCR primers (Invitrogen), and results were analyzed by acrylamide gel electrophoresis. Mice used for the studies described here were speed back-crossed for five generations and displayed >95% C57Bl/6 microsatellite marker loci.

Animals and experimental design

NOX4-deficient and WT male mice aged 10–12 weeks were inbred in specific pathogen-free conditions on the C57BL/6J background. All animal experiments were approved by the Institutional Ethics Committee of Animal Care in Geneva and Cantonal Veterinary Office. Male mice weighing 25–30 g were anesthetized with ketamine and xylazine (100 and 5 mg/kg, respectively) and then placed on an inclined surface below cold light. The larynx was observed below cold light and intubated with an endotracheal catheter attached to a 50-ml Hamilton syringe (Hamilton Bonaduz). Bleomycin (2000 I.U./kg, stock solution prepared at 1000 I.U./ml; Zurich) or vehicle (saline) was instilled to WT and NOX4-deficient male mice. Intubation of the trachea was verified by movement of the solution bubble with the animal's respiratory efforts. After instillation, the catheter was removed, and the mice were returned to their cages, allowed to recover from anesthesia, and provided with free access to food and water. Mice were killed

at days 2, 7, 12, and 21, and lungs processed for subsequent analysis.

Mouse lung histology and immunohistochemistry

The right lung was fixed by intratracheal instillation of 4% PFA and embedded in paraffin. Sections (3 μm) were stained with hematoxylin and eosin or with Masson's Trichrome and examined with light microscopy. For immunohistochemical analysis, sections were incubated with a monoclonal antibody anti α-SMA (mouse IgG2a, 1:400, a kind gift from Prof. G. Gabbiani) (42). Detection was performed using horseradish peroxidase anti-mouse Envision+ system with diaminobenzidine (Dako SA). Sections were then counterstained with hematoxylin.

Sircol assay

Total lung collagen content was determined by measuring total soluble collagen using the Sircol Collagen Assay Kit (Biocolor) at day 21 according to the manufacturer's instructions. Samples were centrifuged at 15,000 *g* and supernatants (100 μl) diluted in 0.5 *M* acid acetic (100 μl), and then 1 ml of Sircol Dye Reagent was added and mixed for 30 min at room temperature in a mechanical shaker. The collagen-dye complex was precipitated by centrifugation at 10,000 *g* for 10 min. The unfixed dye solution was carefully removed. The precipitated complex was resuspended in 1 ml of alkali reagent, and placed in a 96-well flat-bottomed plate; absorbance at 540 nm was evaluated. Collagen content was calculated by comparing samples values to a standard curve.

Western blot analysis

Total lung protein extracts were performed as previously described (34). Proteins blotted on nitrocellulose membrane were incubated with an anti-NOX4 antibody (1:500; Novus Biologicals), an anti-pSmad2 antibody (1:1000; Santa Cruz Biotechnology), an anti-Smad2 antibody (1:1000; Santa Cruz Biotechnology), a specific monoclonal anti-pJNK antibody (1:500; Santa Cruz Biotechnology), a polyclonal JNK (1:1000; Santa Cruz Biotechnology), a monoclonal anti-pERKs (1:1000; Cell Signaling), a polyclonal anti-ERKs (1:1000; Cell Signaling), a polyclonal anti-actin (1:1000; Sigma), and a polyclonal anti-cleaved caspase-3 (1:500; Cell Signaling), followed by incubation with a horseradish peroxidase-conjugated anti-mouse antibody (1:3000; Bio-Rad Laboratories) or peroxidase-conjugated anti-rabbit antibody (1:10,000; Jackson Immunoresearch Laboratories). Proteins were detected by using ECL reagents (Amersham Pharmacia Biotech). Densitometric evaluation was performed using Quantity One software (Bio-Rad Laboratories).

Bronchoalveolar lavage, cell count, and cytokine measurement

At days 2, 7, and 12 after bleomycin instillation, BALF and cell distribution in BALF were performed as described (8). Total cell count was determined using a cell counter. The amounts of IL6 and MCP-1 in the BALF fluids were measured by a Cytometric Bead Array Flex Set System (BD Biosciences).

Alveolar epithelial type II cell isolation

Alveolar type II epithelial cells were isolated from adult mouse (8–14 weeks old) lungs as described with minor modifications (9). Briefly, lungs were inflated with dispase and then placed in 1 ml of dispase while gently agitated at room temperature for 45 min. Lungs were then minced and suspended in 2 ml of dispase containing collagenase (2 μg/ml) and DNase (50 μg/ml). Digested lungs were resuspended in Dulbecco's modified Eagle's medium and 10% fetal calf serum (FCS), and sequentially filtered through 70-, 40-, and 20-μm filters. Cells underwent negative selection using biotinylated anti-CD45 and anti-CD16/32 antibodies (BD Pharmingen) and then separated by streptavidin-coated biomagnetic particle system (Dynabeads; Invitrogen). Epithelial type II cells were cultured either on plastic (less than 24 h) or on chamber slides coated with Matrigel, supplemented with 5% collagen type I and 25% serum free medium for longer experiments. The cells were maintained with 10% FCS in a 37°C incubator, and the medium was replaced after 1 day.

Detection of superoxide

For *in situ* detection, frozen lung tissue from WT and NOX4-deficient mice exposed to saline or bleomycin for 7 days was cryosectioned (20 μM) and collected onto Superfrost plus slides (Menzel GmbH and Co KG) allowed to air-dry at room temperature and stored at −80°C. When needed, slides were placed into phosphate-buffered saline (PBS) for 30 min at room temperature and then stained with DHE (5 μM) diluted in Hank's Balanced Salt Solution for 30 min in the dark. The slides were rinsed extensively with Hank's Balanced Salt Solution and cover-slipped, and the images were captured with an inverted microscope (Nipkow) and analyzed with Metafluor imaging software (Molecular Devices). Quantification was performed by measuring the fluorescence intensity of all nuclei counted in the lung sections from three different mice.

Alveolar epithelial type II cells isolated from WT and NOX4-deficient mice were treated with 10 ng/ml TGF-β_1 for 6 h in Dulbecco's modified Eagle's medium supplemented with 0.05% FCS and stained with 10 μM of DHE (Sigma) diluted in PBS. Images were captured for 30 min with an inverted microscope (Nipkow) and analyzed with Metafluor imaging software (Molecular Devices). Values were obtained by measuring fluorescence intensity on isolated epithelial type II cells (>50 cells for each mouse) from three different mice.

TUNEL assay and immunostaining

Frozen lung sections at days 2, 7, 12, and 21 (6 μm) were fixed by instillation with 4% PFA and permeabilized during 2 min on ice with 0.1% Tx-100 in 0.1% sodium citrate. After blocking with 10% normal goat serum and 1% bovine serum albumin in PBS solution, sections were incubated with an antibody anti-digitoxigenin-AP Fab fragments for 30 min at room temperature (1/500; Roche) as described by the manufacturer (TUNEL assay fluorescent kit; Roche). Fast Red substrate system (DaKo) was used to detect the fluorescent staining and nuclei were revealed with 4,6-diamidino-2-phenylindole (DAPI) (1/200; Roche). Slides were mounted with Mowiol and analyzed by confocal microscopy (LSM 510Meta; Zeiss). Quantification of positive staining was

performed using Metamorph analysis software (20 images per mouse, three mice per group out of three independent experiments).

For double staining, after TUNEL staining according to the manufacturer (TUNEL assay fluorescent kit; Roche), frozen lung sections were washed in PBS and incubated 1 h at room temperature with hamster syrian polyclonal antibody anti-T1alpha (1:1000; Santa-Cruz), rabbit polyclonal anti-prosurfactant C protein (1:250; Chemicon), or anti–Von Willebrand factor (1:250; DAKO). After washing, sections were incubated with a goat anti-syrian hamster Texas red (1:200; Jackson) or a goat anti-rabbit Texas Red conjugated (1:250; Molecular Probe). The nuclei were stained with DAPI (1:200; Roche Diagnostic). Slides were mounted with fluorsave (VWR) and analyzed by confocal microscopy (LSM 510 Meta; Zeiss).

TUNEL detection in isolated cells was performed as described by the manufacturer (TUNEL assay fluorescent kit; Roche). Briefly, isolated epithelial cells from both mice strains were cultured on matrigel and treated with 10 ng/ml TGF-β_1 for 24 h. Cells were fixed with 4% PFA for 1 h at room temperature and then permeabilized during 2 min on ice with 0.1% Tx-100 in 0.1% sodium citrate freshly prepared. Cells were incubated with the labeling mixture, and stained with a rabbit polyclonal anti-prosurfactant protein C (1:250; Chemicon) for 1 h at 37°C. As secondary antibody, a goat anti-rabbit Texas Red conjugated (dilution 1/250; Molecular Probe) was used. The nuclei were stained with DAPI (1/200; Roche Diagnostic). These slides were then mounted with mowiol as described previously. Images were acquired by confocal microscopy (LSM510 Meta; Zeiss) and quantified using Metamorph analysis software (20 images per mouse, three mice per group out of three independent experiments).

Real-time PCR

Spleen, kidney, and pulmonary samples were placed in RNA later (Qiagen). After homogenization with the Tissue Lyser (Qiagen), RNA was extracted with the RNeasy Protect mini kit (Qiagen) and reverse transcribed using the superscript reverse transcriptase (Superscript Choice; Invitrogen). A total of 1 μg of sample was used as a template for the real-time PCR. We used the following primer sequences for Col3a1 (procollagen type III): 5′-ACC CTT CAT CCC ACT CTT ATT T-3′ and 5′-CAT CGT TCT GGC TTC CAG ACA-3′; for NOX4: 5′-CCG GAC AGT CCT GGC TTA TCT-3′ and 5′-TGC TTT TAT CCA ACA ATC TTC TTG TT-3′; for GAPDH, 5′-TCC ATG ACA ACT TTG GCA TTG-3′ and 5′-CAG TCT TCT GGG TGG CAG TGA-3′; and for GusB, 5′-ACG GGA TTG TGG TCA TCG A and 5′-TGA CTC GTT GCC AAA ACT CTG A.

Statistical analysis

Results are expressed as mean ± standard error of the mean and ± standard deviation as indicated and were analyzed either by Wilcoxon Rank test or by analysis of variance, as appropriate. Significance levels were set at $p < 0.05$.

Acknowledgments

The authors would like to thank S. Startchik, O. Plastre, J. Smith-Clerc, and P. Henchoz for technical assistance and Drs. S. Izui, M.L Santiago-Raber, M.L. Bochaton-Piallat, and A. Ait-Lounis, for help and advice. The specific dual NOX4/NOX1 inhibitor, GKT136901, was kindly provided by Genkyotex SA (www.genkyotex.com), Plan-les-Ouates, Geneva, Switzerland. This work was supported by grants from the Swiss National Foundation (to C.B.-A., B.H., and K.H.K.), the Eagle and the Gertrude von Meissner Foundation (to C.B.-A.), and Societé de Pneumologie de Langue Française and Swiss Society for Pneumology (to S.C.), the NIH grant R01 AR0230, and the Jamie Rabinowitch-Davis and the Minsk foundations (to J.L.A).

Author Disclosure Statement

S.C., C.D., Y.D., O.B., B.H., O.P.-S., C.G., B.B., J.L.A., J.-C.P., and C.B.-A.: no competing financial interests exist. K.-H.K is a founding member of the start-up company Genkyotex, which develops NOX inhibitors.

References

1. Alcorn JF, van der Velden J, Brown AL, McElhinney B, Irvin CG, and Janssen-Heininger YM. c-Jun N-terminal kinase 1 is required for the development of pulmonary fibrosis. *Am J Respir Cell Mol Biol* 40: 422–432, 2008.
2. Amara N, Goven D, Prost F, Muloway R, Crestani B, and Boczkowski J. NOX4/NADPH oxidase expression is increased in pulmonary fibroblasts from patients with idiopathic pulmonary fibrosis and mediates TGFbeta1-induced fibroblast differentiation into myofibroblasts. *Thorax* 65: 733–738, 2010.
3. Bedard K and Krause KH. The NOX family of ROS-generating NADPH oxidases: physiology and pathophysiology. *Physiol Rev* 87: 245–313, 2007.
4. Bhandarkar SS, Jaconi M, Fried LE, Bonner MY, Lefkove B, Govindarajan B, Perry BN, Parhar R, Mackelfresh J, Sohn A, Stouffs M, Knaus U, Yancopoulos G, Reiss Y, Benest AV, Augustin HG, and Arbiser JL. Fulvene-5 potently inhibits NADPH oxidase 4 and blocks the growth of endothelial tumors in mice. *J Clin Invest* 119: 2359–2365, 2009.
5. Brown DI and Griendling KK. Nox proteins in signal transduction. *Free Radic Biol Med* 47: 1239–1253, 2009.
6. Budinger GR, Mutlu GM, Eisenbart J, Fuller AC, Bellmeyer AA, Baker CM, Wilson M, Ridge K, Barrett TA, Lee VY, and Chandel NS. Proapoptotic Bid is required for pulmonary fibrosis. *Proc Natl Acad Sci U S A* 103: 4604–4609, 2006.
7. Carnesecchi S Deffert C, Pache JC, Donati Y, Krause KH, and Barazzone-Argiroffo C. NADPH oxidase 4 (NOX4) deficiency protects from bleomycin-induced epithelial cell death and lung fibrosis [abstract]. Barcelonne, Spain: ERS, September 18–22, 2010.
8. Carnesecchi S, Deffert C, Pagano A, Garrido-Urbani S, Metrailler-Ruchonnet I, Schappi M, Donati Y, Matthay MA, Krause KH, and Barazzone Argiroffo C. NADPH oxidase-1 plays a crucial role in hyperoxia-induced acute lung injury in mice. *Am J Respir Crit Care Med* 180: 972–981, 2009.
9. Corti M, Brody AR, and Harrison JH. Isolation and primary culture of murine alveolar type II cells. *Am J Respir Cell Mol Biol* 14: 309–315, 1996.
10. Cucoranu I, Clempus R, Dikalova A, Phelan PJ, Ariyan S, Dikalov S, and Sorescu D. NAD(P)H oxidase 4 mediates transforming growth factor-beta1-induced differentiation of cardiac fibroblasts into myofibroblasts. *Circ Res* 97: 900–907, 2005.

11. Day BJ. Antioxidants as potential therapeutics for lung fibrosis. *Antioxid Redox Signal* 10: 355–370, 2008.
12. Demedts M, Behr J, Buhl R, Costabel U, Dekhuijzen R, Jansen HM, MacNee W, Thomeer M, Wallaert B, Laurent F, Nicholson AG, Verbeken EK, Verschakelen J, Flower CD, Capron F, Petruzzelli S, De Vuyst P, van den Bosch JM, Rodriguez-Becerra E, Corvasce G, Lankhorst I, Sardina M, and Montanari M. High-dose acetylcysteine in idiopathic pulmonary fibrosis. *N Engl J Med* 353: 2229–2242, 2005.
13. Gauldie J, Bonniaud P, Sime P, Ask K, and Kolb M. TGF-beta, Smad3 and the process of progressive fibrosis. *Biochem Soc Trans* 35: 661–664, 2007.
14. Geiszt M, Kopp JB, Varnai P, and Leto TL. Identification of renox, an NAD(P)H oxidase in kidney. *Proc Natl Acad Sci U S A* 97: 8010–8014, 2000.
15. Grandvaux N, Soucy-Faulkner A, and Fink K. Innate host defense: Nox and Duox on phox's tail. *Biochimie* 89: 1113–1122, 2007.
16. Hecker L, Vittal R, Jones T, Jagirdar R, Luckhardt TR, Horowitz JC, Pennathur S, Martinez FJ, and Thannickal VJ. NADPH oxidase-4 mediates myofibroblast activation and fibrogenic responses to lung injury. *Nat Med* 15: 1077–1081, 2009.
17. Hinz B. Formation and function of the myofibroblast during tissue repair. *J Invest Dermatol* 127: 526–537, 2007.
18. Hunninghake GW. Antioxidant therapy for idiopathic pulmonary fibrosis. *N Engl J Med* 353: 2285–2287, 2005.
19. Kang HR, Cho SJ, Lee CG, Homer RJ, and Elias JA. Transforming growth factor (TGF)-beta1 stimulates pulmonary fibrosis and inflammation via a Bax-dependent, bid-activated pathway that involves matrix metalloproteinase-12. *J Biol Chem* 282: 7723–7732, 2007.
20. Kinnula VL, Fattman CL, Tan RJ, and Oury TD. Oxidative stress in pulmonary fibrosis: a possible role for redox modulatory therapy. *Am J Respir Crit Care Med* 172: 417–422, 2005.
21. Koli K, Myllarniemi M, Keski-Oja J, and Kinnula VL. Transforming growth factor-beta activation in the lung: focus on fibrosis and reactive oxygen species. *Antioxid Redox Signal* 10: 333–342, 2008.
22. Kuwano K. Epithelial cell apoptosis and lung remodeling. *Cell Mol Immunol* 4: 419–429, 2007.
23. Kuwano K, Kunitake R, Kawasaki M, Nomoto Y, Hagimoto N, Nakanishi Y, and Hara N. P21Waf1/Cip1/Sdi1 and p53 expression in association with DNA strand breaks in idiopathic pulmonary fibrosis. *Am J Respir Crit Care Med* 154: 477–483, 1996.
24. Laleu B, Gaggini F, Orchard M, Fioraso-Cartier L, Cagnon L, Houngninou-Molango S, Gradia A, Duboux G, Merlot C, Heitz F, Szyndralewiez C, and Page P. First in class, potent, and orally bioavailable NADPH oxidase isoform 4 (Nox4) inhibitors for the treatment of idiopathic pulmonary fibrosis. *J Med Chem* 53: 7715–7730, 2010.
25. Lamacchia C, Palmer G, and Gabay C. Discrimination of C57BL/6J Rj and 129S2/SvPasCrl inbred mouse strains by use of simple sequence length polymorphisms. *J Am Assoc Lab Anim Sci* 46: 21–24, 2007.
26. Lee CG, Cho SJ, Kang MJ, Chapoval SP, Lee PJ, Noble PW, Yehualaeshet T, Lu B, Flavell RA, Milbrandt J, Homer RJ, and Elias JA. Early growth response gene 1-mediated apoptosis is essential for transforming growth factor beta1-induced pulmonary fibrosis. *J Exp Med* 200: 377–389, 2004.
27. Manoury B, Nenan S, Leclerc O, Guenon I, Boichot E, Planquois JM, Bertrand CP, and Lagente V. The absence of reactive oxygen species production protects mice against bleomycin-induced pulmonary fibrosis. *Respir Res* 6: 11, 2005.
28. Massague J. How cells read TGF-beta signals. *Nat Rev Mol Cell Biol* 1: 169–178, 2000.
29. Matsuoka H, Arai T, Mori M, Goya S, Kida H, Morishita H, Fujiwara H, Tachibana I, Osaki T, and Hayashi S. A p38 MAPK inhibitor, FR-167653, ameliorates murine bleomycin-induced pulmonary fibrosis. *Am J Physiol Lung Cell Mol Physiol* 283: L103–L112, 2002.
30. Moeller A, Ask K, Warburton D, Gauldie J, and Kolb M. The bleomycin animal model: a useful tool to investigate treatment options for idiopathic pulmonary fibrosis? *Int J Biochem Cell Biol* 40: 362–382, 2008.
31. Moore BB and Hogaboam CM. Murine models of pulmonary fibrosis. *Am J Physiol Lung Cell Mol Physiol* 294: L152–L160, 2008.
32. Moustakas A and Heldin CH. Dynamic control of TGF-beta signaling and its links to the cytoskeleton. *FEBS Lett* 582: 2051–2065, 2008.
33. Pache JC, Carnesecchi S, Deffert C, Donati Y, Herrmann FR, Barazzone Argiroffo C, and Krause KH. Thickened pulmonary arteries in idiopathic pulmonary fibrosis. *Nat Med* 17: 31–32, 2011.
34. Pagano A, Metrailler-Ruchonnet I, Aurrand-Lions M, Lucattelli M, Donati Y, and Argiroffo CB. Poly(ADP-ribose) polymerase-1 (PARP-1) controls lung cell proliferation and repair after hyperoxia-induced lung damage. *Am J Physiol Lung Cell Mol Physiol* 293: L619–L629, 2007.
35. Pedruzzi E, Guichard C, Ollivier V, Driss F, Fay M, Prunet C, Marie JC, Pouzet C, Samadi M, Elbim C, O'Dowd Y, Bens M, Vandewalle A, Gougerot-Pocidalo MA, Lizard G, and Ogier-Denis E. NAD(P)H oxidase Nox-4 mediates 7-ketocholesterol-induced endoplasmic reticulum stress and apoptosis in human aortic smooth muscle cells. *Mol Cell Biol* 24: 10703–10717, 2004.
36. Rahimi RA and Leof EB. TGF-beta signaling: a tale of two responses. *J Cell Biochem* 102: 593–608, 2007.
37. Reddy MM, Fernandes MS, Salgia R, Levine RL, Griffin JD, and Sattler M. NADPH oxidases regulate cell growth and migration in myeloid cells transformed by oncogenic tyrosine kinases. *Leukemia* 25: 281–289, 2011.
38. Ross S and Hill CS. How the Smads regulate transcription. *Int J Biochem Cell Biol* 40: 383–408, 2008.
39. Selman M, King TE, and Pardo A. Idiopathic pulmonary fibrosis: prevailing and evolving hypotheses about its pathogenesis and implications for therapy. *Ann Intern Med* 134: 136–151, 2001.
40. Serrander L, Cartier L, Bedard K, Banfi B, Lardy B, Plastre O, Sienkiewicz A, Forro L, Schlegel W, and Krause KH. NOX4 activity is determined by mRNA levels and reveals a unique pattern of ROS generation. *Biochem J* 406: 105–114, 2007.
41. Sisson TH, Mendez M, Choi K, Subbotina N, Courey A, Cunningham A, Dave A, Engelhardt JF, Liu X, White ES, Thannickal VJ, Moore BB, Christensen PJ, and Simon RH. Targeted injury of type II alveolar epithelial cells induces pulmonary fibrosis. *Am J Respir Crit Care Med* 181: 254–263, 2010.
42. Skalli O, Ropraz P, Trzeciak A, Benzonana G, Gillessen D, and Gabbiani G. A monoclonal antibody against alpha-smooth muscle actin: a new probe for smooth muscle differentiation. *J Cell Biol* 103: 2787–2796, 1986.

43. Thannickal VJ and Horowitz JC. Evolving concepts of apoptosis in idiopathic pulmonary fibrosis. *Proc Am Thorac Soc* 3: 350–356, 2006.
44. Tomasek JJ, Gabbiani G, Hinz B, Chaponnier C, and Brown RA. Myofibroblasts and mechano-regulation of connective tissue remodelling. *Nat Rev Mol Cell Biol* 3: 349–363, 2002.
45. Uhal BD, Joshi I, Hughes WF, Ramos C, Pardo A, and Selman M. Alveolar epithelial cell death adjacent to underlying myofibroblasts in advanced fibrotic human lung. *Am J Physiol* 275: L1192–L1199, 1998.
46. Waghray M, Cui Z, Horowitz JC, Subramanian IM, Martinez FJ, Toews GB, and Thannickal VJ. Hydrogen peroxide is a diffusible paracrine signal for the induction of epithelial cell death by activated myofibroblasts. *FASEB J* 19: 854–856, 2005.
47. Wang R, Ibarra-Sunga O, Verlinski L, Pick R, and Uhal BD. Abrogation of bleomycin-induced epithelial apoptosis and lung fibrosis by captopril or by a caspase inhibitor. *Am J Physiol Lung Cell Mol Physiol* 279: L143–L151, 2000.
48. Weyemi U, Caillou B, Talbot M, Ameziane-El-Hassani R, Lacroix L, Lagent-Chevallier O, Al Ghuzlan A, Roos D, Bidart JM, Virion A, Schlumberger M, and Dupuy C. Intracellular expression of reactive oxygen species-generating NADPH oxidase NOX4 in normal and cancer thyroid tissues. *Endocr Relat Cancer* 17: 27–37, 2010.
49. Wynn TA. Cellular and molecular mechanisms of fibrosis. *J Pathol* 214: 199–210, 2008.
50. Xaubet A, Marin-Arguedas A, Lario S, Ancochea J, Morell F, Ruiz-Manzano J, Rodriguez-Becerra E, Rodriguez-Arias JM, Inigo P, Sanz S, Campistol JM, Mullol J, and Picado C. Transforming growth factor-beta1 gene polymorphisms are associated with disease progression in idiopathic pulmonary fibrosis. *Am J Respir Crit Care Med* 168: 431–435, 2003.

Address correspondence to:
Dr. Stephanie Carnesecchi
Department of Pathology and Immunology
Medical School
University of Geneva
1 rue Michel Servet
1211 Geneva 4
Switzerland

E-mail: stephanie.carnesecchi@unige.ch

Date of first submission to ARS Central, December 7, 2010; date of final revised submission, March 9, 2011; date of acceptance, March 10, 2011.

Abbreviations Used

α-SMA = α-smooth muscle actin
BALF = bronchoalveolar lavage fluid
BLM = bleomycin
DAPI = 4,6-diamidino-2-phenylindole
DHE = dihydroethidium
FCS = fetal calf serum
IPF = idiopathic pulmonary fibrosis
PBS = phosphate-buffered saline
PCR = polymerase chain reaction
PFA = paraformaldehyde
ROS = reactive oxygen species
TGF = transforming growth factor
WT = wild-type